

Sub-threshold channels at the edges of nano-scale triple-gate silicon transistors

H. Sellier,* G. P. Lansbergen, J. Caro, and S. Rogge

Kavli Institute of Nanoscience, Delft University of Technology, Lorentzweg 1, 2628 CJ Delft, The Netherlands

N. Collaert, I. Ferain, M. Jurczak, and S. Biesemans

InterUniversity Microelectronics Center (IMEC), Kapeldreef 75, 3001 Leuven, Belgium

We investigate by low-temperature transport experiments the sub-threshold behavior of triple-gate silicon field-effect transistors. These three-dimensional nano-scale devices consist of a lithographically defined silicon nanowire surrounded by a gate with an active region as small as a few tens of nanometers, down to $50 \times 60 \times 35 \text{ nm}^3$. Conductance versus gate voltage show Coulomb-blockade oscillations with a large charging energy due to the formation of a small potential well below the gate. According to dependencies on device geometry and thermionic current analysis, we conclude that sub-threshold channels, a few nanometers wide, appear at the nanowire edges, hence providing an experimental evidence for the corner-effect.

Non-planar field effect transistors called FinFETs [1] are currently being developed to solve the problematic issues encountered with the standard planar geometry when the channel length is reduced to a sub-100 nm size. Their triple-gate geometry is expected to have a more efficient gate action and to solve the leakage problem through the body of the transistor, one of the dramatic short channel effects [2]. However, their truly 3-dimensional (3D) structure makes doping—and thus also potential—profiles very difficult to simulate and to understand using the current knowledge on device technology. Transport studies at low temperature, where the thermally activated transport is suppressed, can bring insight to these questions by measuring local gate action. For this reason we experimentally investigate the potential profile by conductance measurements and observe the formation of a sub-threshold channel at the edge of the silicon nanowire. This corner effect has been proposed [3, 4] as an additional contribution to the sub-threshold current in these 3D triple-gate structures where the edges of the nanowire experience stronger gate action due to geometric enhancement of the field. However, besides extensive simulation work [3, 4]—keeping in mind the difficulties with these 3D structures—very little experimental work has been published until now on this effect [5].

The FinFETs discussed here consist of a narrow single-crystalline silicon wire with two large contact pads etched in a p-type Silicon On Insulator (SOI) layer doped with 10^{18} cm^{-3} boron atoms. This silicon wire is covered with a $t_{\text{ox}} = 1.4 \text{ nm}$ thick thermal oxide and a second narrow poly-crystalline silicon wire crossing the first one is fabricated to form a gate that surrounds the wire on three faces (Fig. 1(a)). The entire surface is then implanted with 10^{19} cm^{-3} arsenic atoms to form n-type degenerate source, drain, and gate. During this implantation

the wire located below the gate is protected and remains p-type. In the investigated device series the height of the fin wire is $H = 60 \text{ nm}$, while the width ranges from $W = 35 \text{ nm}$ to $1 \mu\text{m}$ and the gate length ranges from $L = 50 \text{ nm}$ to $1 \mu\text{m}$. The relatively high p-type doping of the channel wire is chosen to ensure a depletion length shorter than half the channel length in order to have a fully developed potential barrier in this n-p-n structure and so to keep the conductance threshold at a large enough positive gate voltage. The characteristics at room temperature of these nano-scale FinFETs look therefore similar to those of their larger planar counterparts (Fig. 1(b) at 300 K).

For sub-threshold voltages, a barrier exists between the source and drain electron reservoirs and the transport is thermally activated at high enough temperature as shown in Fig. 2(b). For very short devices, the conductance is simply given by the thermionic emission above the barrier according to the formula:

$$G = S A^* T (e/k_B) \exp(-E_b/k_B T)$$

where the effective Richardson constant A^* for Si is $2.1 \times 120 \text{ A cm}^{-2} \text{ K}^{-2}$ [6]. Several samples have been mea-

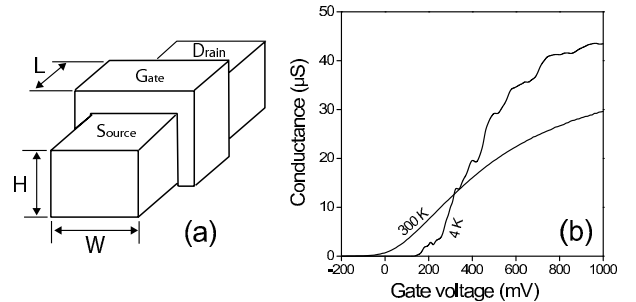


FIG. 1: (a) Schematic of the FinFET geometry where the gate surrounds the Si nanowire (the fin). (b) Low bias conductance versus gate voltage for a long and narrow silicon FinFET ($L = 950 \text{ nm}$, $W = 35 \text{ nm}$) at room and liquid helium temperatures. Reproducible conductance fluctuations appear due to quantum interferences.

*Present address: Laboratoire de Spectrométrie Physique, UJF-CNRS Grenoble, France. Electronic mail: hermann.sellier@ujf-grenoble.fr

sured in this regime and their conductance has been fitted to obtain the barrier height E_b and the cross section S (Fig. 2(d)). The two 385 nm wide samples have the same cross section $S \approx 4 \text{ nm}^2$ although their length differ by a factor 2. We can therefore conclude that transport is dominated by thermionic emission. The two 135 nm wide samples however have different S values, but this can not imply a diffusive transport since the longest sample has the largest conductance. Another result is that the cross section $S \approx 4 \text{ nm}^2$ is much smaller than the channel width W (135 or 385 nm) multiplied by the channel thickness (about 1 nm). This result is consistent with the corner-effect that produces a lower conduction band (stronger electric field) along the two edges of the wire, where the current will therefore flow preferentially (Fig. 3(b)). This interpretation is confirmed by the result obtained on a 385 nm wide sample with an undoped channel. Its larger cross section $S = 24 \text{ nm}^2$ (still much smaller than the width) is in agreement with the corner-effect since the longer depletion length of the undoped silicon gives smoother potential variations and therefore wider channels along the edges.

The barrier height E_b versus gate voltage is plotted in Fig. 2(c). The data extrapolated to zero gate voltage are consistent with a 220 meV barrier height calculated for a p-type channel in contact with a n^{++} gate through a 1.4 nm SiO_2 dielectric [6]. The linear dependence of the barrier height shows a good channel/gate coupling ratio $\alpha = dE_b / e dV_G = 0.68$ due to the triple gate geometry with a thin gate oxide. At higher gate voltage (above 300 mV) the coupling ratio decreases and a finite barrier survives up to large voltages. Analysis of the low tem-

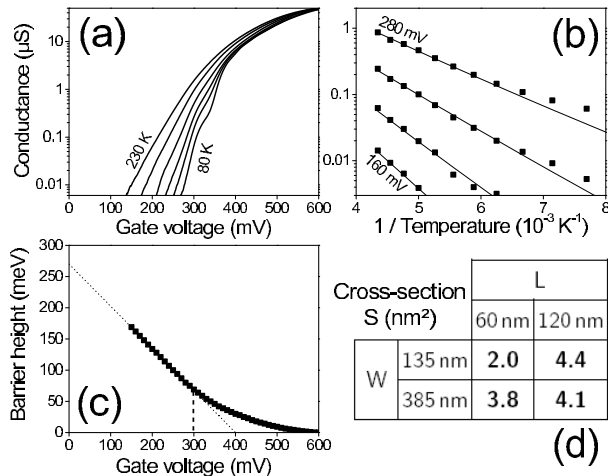


FIG. 2: (a) Conductance versus gate voltage (30 K steps) for a short and wide fin ($L = 60 \text{ nm}$, $W = 385 \text{ nm}$). (b) Conductance plotted versus the inverse of the temperature (40 mV steps) for the same sample. The conductance is thermally activated above 150 K. (c) Barrier height versus gate voltage changing behavior at 300 mV (same sample). (d) Measured cross-section S for the activated current of 4 samples with different length L and width W .

perature transport (see below) shows however that the gate action remains constant inside the channel where localized states are formed. The finite barrier is in fact two confining barriers located in the access regions (between channel and contacts) where the concentration of implanted arsenic atoms is reduced by the masking silicon nitride spacers placed next to the gate (Fig. 3(a)).

At low temperature the conductance develops fluctuations versus gate voltage (see Fig. 1(b)) with a pattern that reproduces after thermal cycling (at least for the main features). These fluctuations are caused by quantum interferences in the channel. For gate voltages close to the threshold, charge localization occurs, especially for short fins as can be seen in Fig. 3(c). When cooled down to 4.2 K the conductance pattern develops a series of peaks that we attribute to Coulomb blockade of electrons in the potential well created in the channel by the two tunnel barriers of the low-doped access regions [7, 8]. This interpretation is supported by the channel-length dependence of the peak spacing discussed later. An explanation in terms of a quantum well formed by an impurity can be ruled out. An impurity or defect could not accept many electrons, e.g. more than 20 for the 100 nm sample in Fig. 4(b), since they represent a single charge or empty state. These devices act therefore as quantum dots where the conduction electrons are spatially localized and are Coulomb blocked for the transport by a finite charging energy [9].

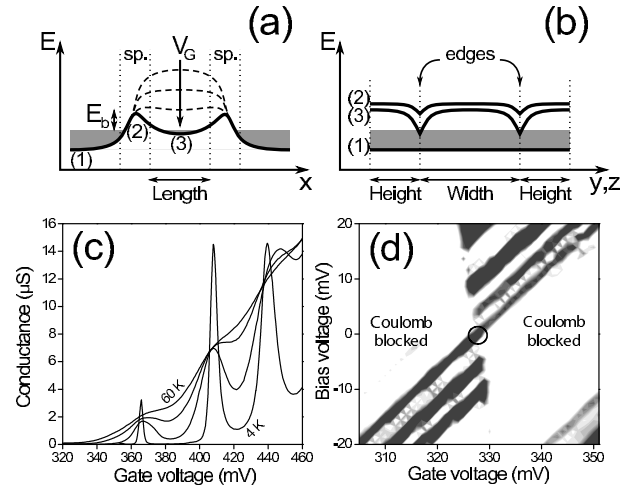


FIG. 3: (a) Conduction band edge profile with the highest barrier in the channel or in the access regions below the spacers (sp.) depending on gate voltage. (b) Band edge along the 3D gate oxide interface (1) in the contacts, (2) in the barriers, (3) in the channel. The corner-effect produces two channels with low barriers at the wire edges. (c) Conductance versus gate voltage for a short and wide channel ($L = 60 \text{ nm}$, $W = 385 \text{ nm}$) showing Coulomb blockade peaks up to high temperatures (20 K steps). (d) Stability diagram, i.e. conductance versus gate and bias voltages, at 4.2 K. The circle indicates a zero bias conductance peak, which develops into a triangular sector at finite bias.

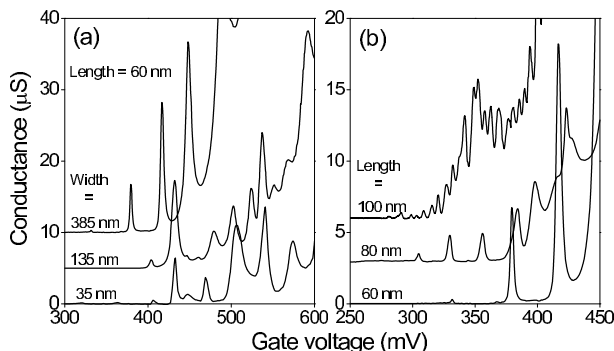


FIG. 4: Conductance versus gate voltage at 4.2 K for several devices. (a) Short fins ($L = 60$ nm) of different widths ($W = 35, 135, 385$ nm) have a similar peak spacing. (b) Devices with longer fins ($L = 60, 80, 100$ nm) have a smaller peak spacing (the widths are different). The curves have been shifted for clarity.

In the stability diagram of a quantum dot (see Fig. 3(d)), the slopes of a triangular conducting sector give the ratios of the capacitances C_G , C_S , and C_D between the dot and respectively the gate, source, and drain electrodes [9]. In this way we find the dot/gate coupling $\alpha = C_G/(C_G + C_S + C_D) = 0.78$ (0.65) for the first (second) resonance. These values are close to the channel/gate coupling 0.68 obtained independently in the same sample from the gate voltage dependence of the barrier height in the middle of the channel at higher temperatures. This result indicates that the gate coupling in the center of the device remains constant and supports the idea of a minimum in the conduction band as sketched in Fig. 3(a).

The peak spacing ΔV_G is the change in gate voltage that increases by one the number of electrons in the dot located at the silicon/oxide interface. This quantity provides the dot/gate capacitance $C_G = e/\Delta V_G$, and then the dot area $S = C_G/C_{ox}$ using the gate capacitance per unit area $C_{ox} = \epsilon_{ox}/t_{ox} = 0.025$ F/m². The peak spacings for the same gate length ($L = 60$ nm) but three different channel widths ($W = 35, 135, 385$ nm) can be compared in Fig. 4(a). Although the patterns are not very regular, an average peak spacing of about 30 mV is obtained for all of them, indicating similar dot areas whereas the effective width is varied by more than a fac-

tor three. On the opposite, the conductance patterns for three different lengths ($L = 60, 80$, and 100 nm) shown in Fig. 4(b) have decreasing average peak spacings ($\Delta V_G = 39, 24$, and 6 mV respectively) and therefore increasing dot areas ($S = 160, 270$, and 1100 nm²). However these areas are not strictly proportional to the gate length, so that the actual width could be length dependent or the actual dot length could be smaller than the gate length for very short fins. If we assume that the dot length equals the gate length, we obtain 2.7, 3.4, and 11 nm for the dot width, *i.e.* a small fraction of the total Si/oxide interface width $W_{eff} = W + 2H = 150$ to 500 nm. The observation of similar dot widths of a few nm for different fin widths of hundreds of nm is consistent with the idea of a dot located at the edge of the fin and thus with the corner effect [3, 4].

In addition to a large charging energy $E_c = \alpha e \Delta V_G$, these dots also have a large quantum level spacing ΔE as can be deduced from the temperature dependence of the conductance peaks in Fig. 3(c). When the temperature is lowered below the level spacing, the tunneling process involves a single quantum level at a time and the peak height starts to increase above the high temperature value [10]. The crossover from the classical to the quantum regime of Coulomb blockade being around 15 K, we estimate the level spacing to be about 1.3 meV. If we use the gate length $L = 60$ nm in the expression $\Delta E = 3\pi^2\hbar^2/2m^*L^2$ for the energy separation between the first and second states of a 1D system, we find a level spacing $\Delta E = 1.6$ meV similar to the experimental estimation. This result supports the idea of a long dot extending over the whole gate length (assumed above to extract the dot width from the dot/gate capacitance).

In conclusion, both the activated current amplitude, the Coulomb blockade peak spacing, and the quantum level spacing reveal that the current flows in narrow channels a few nanometers wide. They appear along the edges of the FinFET due to an enhanced band-bending called corner-effect. In order to get an homogeneous current distribution with a lower sub-threshold current and a larger on/off current ratio, this effect should be reduced. Better devices would have rounder corners on the scale of the depletion length and a lower doping concentration in the channel.

-
- [1] D. Hisamoto, W.-C. Lee, J. Kedzierski, H. Takeuchi, K. Asano, C. Kuo, E. Anderson, T.-J. King, J. Bokor, and C. Hu, *IEEE Trans. Elec. Dev.* **47**, 2320 (2000).
 - [2] M.C. Lemme, T. Mollenhauer, W. Henschel, T. Wahlbrink, M. Baus, O. Winkler, R. Granzner, F. Schwier, B. Spangenberg, and H. Kurz, *Solid-State Electronics* **48**, 529 (2004).
 - [3] B.S. Doyle, S. Datta, M. Doczy, S. Hareland, B. Jin, J. Kavalieros, T. Linton, A. Murthy, R. Rios, and

- R. Chau, *IEEE Elec. Dev. Let.* **24**, 263 (2003).
- [4] J.G. Fossum, J.-W. Yang, and V.P. Trivedi, *IEEE Elec. Dev. Let.* **24**, 745 (2003).
- [5] W. Xiong, J.W. Park, and J.P. Colinge, *IEEE Elec. Dev. Let.* **25**, 541 (2004).
- [6] S. Sze, in *Physics of Semiconductor Devices*, 2nd ed., p. 257 (Wiley, New York, 1981).
- [7] F. Boeuf, X. Jehl, M. Sanquer, and T. Skotnicki, *IEEE Trans. Nanotech.* **2**, 144 (2003).

- [8] X. Jehl, M. Sanquer, G. Bertrand, G. Guegan, S. Deleonibus, and D. Fraboulet, IEEE Trans. Nanotech. **2**, 308 (2003).
- [9] L.P. Kouwenhoven, C.M. Marcus, P.L. McEuen, S. Tarucha, R.M. Westervelt, and N.S. Wingreen, in *Mesoscopic Electron Transport*, Proceedings of the NATO Advanced Study Institutes, vol. 345, p. 105 (Kluwer, Dordrecht, 1997).
- [10] C. W. J. Beenakker, Phys. Rev. B **44**, 1646 (1991).